Label-free immunodetection of α-synuclein by using a microfluidics coplanar electrolyte-gated organic field-effect transistor.

Simona Ricci[1], Stefano Casalini[1,2,], Vitaliy Parkula[3,4,§], Meenu Selvaraj[3], Gulseren Deniz Saygin[3], Pierpaolo Greco[3], Fabio Biscarini[4,5], Marta Mas-Torrent[1,*]*

[1]Institut de Ciència de Materials de Barcelona (ICMAB-CSIC), Networking Research Center on Bioengineering, Biomaterials and Nanomedicine (CIBER-BBN), Campus de la Universitat Autònoma de Barcelona, Cerdanyola, 08193, Barcelona, Spain.

[2]Department of Chemical Sciences, University of Padua,via Francesco Marzolo 1, 35131, Padova, Italy.

[3]Scriba Nanotecnologie srl, via di Corticelli 183/8, 40128, Bologna, Italy.

[4] University of Modena and Reggio Emilia,Via G. Campi 103, 41125 Modena, Italy

[5] Center for Translational Neurophysiology - Istituto Italiano di Tecnologia, Via Fossato di Mortara 17-19, 44100 Ferrara,Italy

[§]Current address: Istituto Sintesi Organica e Fotoreattività (ISOF - CNR), Via P. Gobetti, 101, 40129, Bologna, Italy.

**E-mail: mmas@icmab.es; stefano.casalini@unipd.it*

Abstract

The aggregation of α-synuclein is a critical event in the pathogenesis of neurological diseases, such as Parkinson or Alzheimer. Here, we present a label-free sensor based on an Electrolyte-Gated Organic Field-Effect Transistor (EGOFET) integrated with microfluidics that allows us to detect amounts of α-synuclein in the range from 0.25 pM to 25 nM. The lower limit of detection (LOD) measures the potential of our integrated device as a tool for prognostics and diagnostics. In our device, the gate electrode is the effective sensing element as it is functionalized with anti-(α-synuclein) antibodies using a dual strategy: i) an amino-terminated self-assembled monolayer activated by glutaraldehyde, and ii) the His-tagged recombinant protein G. In both approaches, comparable sensitivity values were achieved, featuring very low LOD values at the sub-pM level. The microfluidics engineering is central to achieve a controlled functionalization of the gate electrode and avoid contamination or physisorption on the organic semiconductor. The demonstrated sensing architecture, being a disposable stand-alone chip, can be operated as a point-of-care test, but also it might represent a promising label-free tool to explore *in-vitro* protein aggregation that takes place during the progression of neurodegenerative illnesses.

Keywords

Biosensing chip, alpha-synuclein, electrolyte-gated organic field-effect transistors, microfluidics

1. Introduction

α-synuclein is a small protein formed by 140 amino acids (19-20 kDa), which, in its pathological condition, is a component of the so-called Lewy Body inclusions. This protein has been considered as a possible hallmark of a group of neurodegenerative diseases, known as *synucleinopathies*, which include Parkinson's disease (PD), the second most common neurodegenerative disease (Chang et al., 2020; Goedert et al., 2017; Gould et al., 2014; Spillantini and Goedert, 2000). Furthermore, α-synuclein has also been shown to play a role in the pathophysiology of Alzheimer's disease (AD) (Twohig and Nielsen, 2019; Wennström et al., 2013). Specifically for PD, there are still no conclusive results about the correlation between the specific levels of circulating α-synuclein in plasma and cerebrospinal fluid (CSF) with the clinical diagnosis and progression of this illness, which has been mainly accounted by variations in the assays detection and sensitivity/accuracy (Bougea et al., 2019; Shi et al., 2010). Thus, the development of highly sensitive devices able to detect this protein in the range from nM down to pM is required for the diagnosis and prognostics of PD and the understanding of the correlation of the α-synuclein levels on its evolution.

Label-free immunosensors that exploit an organic semiconductor channel as the transducer of the biorecognition events are emerging as ultrasensitive and highly specific devices for bioanalytical assays, with figures of merit often comparable, sometimes even superior (with levels of detection down to a few target molecules), to those characterizing the workhorse of bioanalytical techniques viz. the enzyme-linked immunosorbent assays (ELISA) (Engvall and Perlmann, 1971). In comparison to label-free electronic sensors based on inorganic semiconductors, as CHEM-FETs (i.e., chemical field-effect transistors (Kaisti, 2017)) or MOSFETs (i.e., metal-oxide field-effect transistors (Guo et al., 2015)), organic biosensors offer other important advantages, such as the

closer proximity with the aqueous environment (the organic semiconductor channel is immersed in the biologically relevant fluid), the stability of operations in aqueous electrolytes (the typical hysteresis and bias stress observed in ambient operations of organic electronics devices disappear in the liquid environment), the possibility to be interfaced or integrated as arrays with living systems, thanks to the large-area manufacturing on flexible substrates and a suitable bio/functional interface.

Two main device architectures are used for organic transistors as biosensors in aqueous liquids: i) electrolyte-gated organic field-effect transistors (EGOFETs) (Kergoat et al., 2010) and ii) organic electrochemical transistors (OECTs) (Loïg Kergoat et al., 2012). EGOFETs rely on the capacitive coupling between the gate electrode and the active material, whereas OECTs exploit the ion diffusion along with the electrochemical doping of the active material (Rivnay et al., 2018). Relevant bio-applications include electroceuticals (Jonsson et al., 2016), bioelectric signal recording (Campana et al., 2014; Cramer et al., 2013), neuromorphic devices (Desbief et al., 2016; Van De Burgt et al., 2017), and biosensors (Casalini et al., 2015, 2013; Parkula et al., 2020; Wang et al., 2019).

In the case of EGOFET biosensors, the functionalization with a biorecognition group can be done either at the gate electrode (Casalini et al., 2013), or at the organic semiconductor channel (Torsi et al., 2013, 2008). Magliulo et al. (Magliulo et al., 2016) successfully demonstrated both physisorption and chemical grafting of sensing receptors onto the semiconducting channel achieving excellent results towards the quantification of streptavidin and C-reactive protein in a wide range of concentrations, namely from 1 μM to 10 nM and from 2 μM to 2 pM, respectively. However, the approach exerted by using a functionalized gate is generally more convenient, because it avoids the surface engineering of the organic semiconductor, which can affect its

electrical properties and stability during the aqueous operation. As a result, a number of metal functionalization strategies have been successfully demonstrated such as the grafting of antibodies/aptamers mediated either by the Protein G or by self-assembled monolayers (SAMs) (Berto et al., 2019, 2016; Casalini et al., 2015; Magliulo et al., 2016, 2013; Torsi et al., 2013; Wang et al., 2019). The ultimate achievement was the effective detection down to single-molecule of immunoglobulins G/M by co-functionalizing the gate electrode with a SAM endowed with hydrogen-bonding interactions that amplify the individual biorecognition event by a cooperative reorientation of the SAM (Macchia et al., 2018). As the limits of detections are pushed down to such low concentrations, and since many relevant biomarkers, even when overexpressed, are present at extremely low concentration during their patho-physiological condition (*e.g.* inflammatory cytokines), it is crucial to guarantee the electrical stability in these label-free devices. This is particularly important aiming at a new generation of biosensing point-of-care (POC) systems or early diagnostic tools for the detection of relevant biomarkers. Thus, the effort on engineering the optimal interface immunochemistry must be paralleled by the effort in endowing the sensor with compact microfluidics able to guarantee the required stability of parameters during the measurement. The success of such microfluidics has been extensively explored in other types of label-free devices such as the electrochemical (Guo, 2016; Huang et al., 2019) as well as optical ones, (Xu et al., 2019; Zeng et al., 2019). These excellent examples share the same goal, namely a compact chip to be used as a POC test (Xu et al., 2018).

Here, we report on an α-synuclein label-free sensor based on an EGOFET as electronic transduction, whose gate electrode is functionalized by a monoclonal anti-(α-synuclein) antibody. Two different surface functionalization strategies to graft the anti-(α-synuclein) antibody (i.e. SAM and Protein G) are explored. The EGOFET sensor is integrated into a novel microfluidics

layout designed *ad-hoc* to standardize the measurements. This microfluidics consists of separately accommodating the gate and the organic semiconductor, thereby avoiding cross-contamination during the sample dispensing, even though their electrical connection is always preserved for its proper operation. Additionally, the microfluidic is crucial to avoid the fast evaporation of solvent/water, which would produce a temporal drift of the target concentration and hence of the relevant electrochemical potentials in the device. The microfluidic embedded EGOFET featuring a coplanar gate reaches a sensitivity up to 37(±5) mV/dec and a limit-of-detection (LOD) as low as 0.25 pM in phosphate buffered saline (PBS) solution at pH= 7.2 performing analytical tests that take only a few minutes.

2. Materials and methods

2.1. Materials

Human α-synuclein, glutaraldehyde (25% wt), potassium chloride, sodium phosphate dibasic, iron(III) ferrocyanide, polystyrene (MW 10000 g/mol), chlorobenzene, 2,3,4,5,6-pentafluorothiophenol, dextran (from Leuconostoc Mesenteroides, MW= 64.000-76.000 g/mol), and gold wire (Ø 0.5 mm) were purchased from Sigma Aldrich. Sodium chloride and glycerol were purchased from Panreac Quimica. Recombinant His-tagged Protein G was obtained from BioVision, Inc. HS–$(CH_2)_{11}$–$(OCH_2CH_2)_6$–NH_2·HCl (abbreviated as $HSC_{11}EG_6NH_2$) was purchased from ProChimia Surfaces. The anti-(α-synuclein) antibody α-synuclein(211) was purchased from Santa Cruz Biotechnology, Inc. The organic semiconductor, 2,8-Difluoro-5,11-bis(triethylsilylethynyl)anthradithiophene (diF-TES-ADT), was obtained from Lumtec. Acetone and isopropanol were purchased from Chem-Lab and used without further purification. *Kapton®* foils were bought from DuPont (*Kapton®HN*, 75 μm thick). Qsil216 A/B (polydimethylsiloxane, PDMS) was purchased from Farnell Componentes.

2.2. Electrochemistry setup

Electrochemical characterization of the sensing platform was realized with a potentiostat/galvanostat Autolab (PGSTAT128N). The measurements were carried out in a standard three-electrode configuration cell by using Pt, Ag/AgCl, and Au as the counter, reference, and working electrode, respectively.

Electrochemical Impedance Spectroscopy (EIS) was recorded between 0.1 MHz to 0.1 Hz with an AC amplitude equal to 10 mV. The setpoint voltage was the redox potential of the ferricyanide probe. The impedance response was fitted by means of Randles circuit, whose components are the solution resistance (R_s) in series with the charge transfer resistance (R_{CT}) and the Warburg element (W), whereas in parallel the double-layer capacitance (C_{dl}) (Bard and Faulkner., 2002).

Cyclic voltammetry (CV) was measured at different scan rates (10 mV/s, 30 mV/s, 60 mV/s, 90 mV/s, 100 mV/s, 200 mV/s, 300 mV/s, 400 mV/s, 500 mV/s), sweeping the potential from -0.1 V to 0.45 V. Differential Pulse Voltammetry (DPV) was recorded sweeping the potential from -0.1 V to 0.5 V, at a sweep rate equal to 10 mV/s and its modulation amplitude equal to 25 mV. For the reductive desorption of thiols from Au surface, DPV was recorded sweeping the potential from -0.1 V to -1.4 V in NaOH 1 M.

The whole batch of electrochemical measurements was performed in an aqueous solution containing $K_3[Fe(CN)_6]$ 5 mM, KCl 100 mM, and 50 mM of sodium phosphate buffer. The different pHs were adjusted by using small aliquots of NaOH or HCl 1 M. The non-faradaic measurements were carried out in a solution of KCl (100 mM) and sodium phosphate (50 mM) at pH 7.2.

2.3. X-Ray Photoelectron Spectroscopy

XPS measurements were performed at room temperature with a SPECS PHOIBOS 150 hemispherical analyzer (SPECS GmbH, Berlin, Germany) in a base pressure of $5x10^{-10}$ mbar using monochromatic Al K-alpha radiation (1486.74 eV) as the excitation source.

2.4. Surface Plasmon Resonance

For the characterization of the bio-functionalized Au surface by means of Surface Plasmon Resonance (SPR) technique, it was used a SPR platform (*Sensia ß-SPR*), that employs the Kretschmann configuration and incorporates two flow cells (300 nL each) for an independent analysis. The sample is a 1 cm^2 gold chips (2 nm Cr, 50 nm Au), whereas the whole setup works in a semi-automated way. The flow rate was set at 25 µL/min. The sensor surface was excited with a 670 nm light source. Gold chips were cleaned according to the following protocol: sonication in Acetone, EtOH, and bidistilled water for 1 min respectively. The final step consisted of exposing the surface to the UV Ozone cleaner for 30 minutes. All the functionalization steps were carried out *in-situ* and measured in real-time except for the amino-terminated thiols adsorption, which was carried out *ex-situ* because of the incompatibility of the microfluidics tubes with EtOH.

2.5. Device fabrication and measurement

The substrate used for EGOFETs fabrication was *Kapton®*. Source, Drain, and Gate electrodes when required, were patterned by positive photolithography. A thin layer of Au was evaporated, namely 5 nm of Cr (as an adhesive layer) and 40 nm of Au. The channel length (*L*) and width (*W*) were fixed to 30 µm and 18400 µm (i.e. *W/L* ratio equal to 613) respectively. After the metal deposition, the substrates were cleaned by sonication in acetone and isopropanol. The devices were

then exposed to UV Ozone cleaner for 25 minutes. Subsequently, the chip was immersed in a solution of 2,3,4,5,6-pentafluorothiophenol (PFBT, 2 μL/mL in isopropanol) for 15 minutes to functionalize the gold source-drain contacts, rinsed with isopropanol and dried over N_2. In the devices with the coplanar gate electrode, before the source-drain PFBT functionalization, the planar gate electrode was passivated by a thick coating of dextran (*i.e.* drop-casting of a dextran solution 10 mg/mL) (Leonardi et al., 2018). Such a sacrificial layer was removed by immersing the device in water after the deposition of the organic semiconductor in order to leave the gate electrode uncovered.

The organic semiconductor deposition method selected was the so-termed Bar-Assisted Meniscus Shearing (BAMS) (Temiño et al., 2016). A blend of 2,8-Difluoro-5,11-bis(triethylsilylethynyl)anthradithiophene (diF-TES-ADT) and polystyrene Mw= 10000 g/mol (*viz.* PS_{10k}) was dissolved in chlorobenzene 2% wt with a ratio of 4:1. The solution was deposited at 10 mm/s and 105 ºC as previously reported. (Zhang et al., 2016)

The electrical characterization was performed by using a two-channel Keithley Source Meters 2400 and 2601 controlled with a homemade Matlab script, under ambient temperature and dark condition. The device was conditioned by applying V_{GS} = -0.1 V and V_{DS} = -0.1 V until the I_{DS} reached a steady state. Afterwards, transfer characteristics were recorded in the linear regime. For each functionalization step at least three transfers were measured in PBS 0.01x at physiological pH.

2.6. Ex-situ bio-functionalization of the Au wires surfaces and sensing measurements for the top-gated EGOFETs

The polycrystalline Au wire was cleaned according to the following protocol: (i) immersion in NaOH 1 M, heating at above 100 °C for 15 minutes, (ii) immersion in concentrated H_2SO_4 heating at above 100 °C for 15 minutes, (iii) Au electropolish by sweeping the potential from -0.1 V to 1.6 V (15 cycles in H_2SO_4 1 M, as solvent). The functionalization protocols for approach I consisted of the following steps:

(i) incubation in the solution of $HSC_{11}EG_6NH_2$ (1 mM EtOH) at 4 °C overnight. The Au wire was successively rinsed with EtOH and bidistilled water and dried by N_2 flow.

(ii) Activation of the amino-group by dipping the $HSC_{11}EG_6NH_2$-coated wire in a solution of glutaraldehyde (2.5% wt in water) at 4°C for 1 h, and successively rinsed with bidistilled water.

(iii) Incubation into the antibody solution (40 μg/mL in PBS 1x pH 7.2) at RT for 15 minutes.

Approach II relies on the following steps:

(i) Incubation in Recombinant His-tag protein G solution (140 μg/mL in PBS 1x pH 5.5) at RT for 15 minutes.

(ii) Incubation into the anti-(α-synuclein) antibody solution (40 μg/mL in PBS 1x pH 5.5) at RT for 15 minutes.

The α-synuclein solutions were prepared by subsequent dilution starting from 1 mg/mL concentration in PBS 1x pH 7.2. The Ab-coated Au surfaces were incubated for 15 minutes at R.T. with α-synuclein solutions of increasing concentrations in the range from 0.25 pM to 250 nM, and finally abundantly rinsed with PBS 1x pH 7.2 before measurements.

2.7. Microfluidics fabrication for coplanar gate electrode devices

The microfluidic device was constituted by two main parts: i) the inner chamber in Polydimethylsiloxane (PDMS) which contains the PBS solution and ii) the outer holder that serves as a support for the *Kapton®* substrate and properly fixes the PDMS chamber on it. In order to fabricate the chamber and the holder, 3D drawings were made using *SketchUp 2017* software (see Supporting Information, Fig.S1). A master for the PDMS chamber and the holder were printed by means of Digital Light Processing (DLP) 3D printer model "B9Creator V1.2HD". The resin of choice was "B9R-2-Black". A *Sylgard® 184* silicone elastomer was used to create a liquid solution of PDMS and was deposited over the 3D printed mould and cured in oven at 70 °C for 12 h. When the curing process was finished, PDMS microfluidic chamber was removed from the mould and fixed over the planar electrodes on the *Kapton®* substrate. It features a microfluidic channel of 500 μm height and a flexible channel connecting both chambers.

2.8. Functionalisation of the coplanar Au-gate by using the microfluidics and subsequent sensing experiments with the coplanar gate EGOFETs

The self-assembled monolayer formation on the coplanar gate electrode was carried out *ex-situ* by PDMS-assisted printing technique (Leonardi et al., 2018). Afterwards, the microfluidics setup was assembled and the chambers were filled with the electrolyte solution from *Inlet*, employing a peristaltic pump from Watson-Marlow (400 series pump). At this point, activation of the SAM amino-groups by glutaraldehyde (100 μL, 2.5% v/v) and subsequent Ab (50 μL, 40 μg/ml) immobilization was performed *in-situ,* by injecting the corresponding solutions from *Inlet2* at a flow rate equal to 10 μl/min, connecting simultaneously a peristaltic pump at the *Outlet* to pump out the same fluid. Then, buffer solution (PBS 1mM) was injected at 10 μl/min through Inlet2 in order to wash away physisorbed biomolecules, approximatively for 5 minutes.

The subsequent α-synuclein sensing was performed *in-situ*, by injecting the solution containing the receptors (50 μl) at a flow rate of 10 μl/min from *Inlet2*, for about five minutes. After each functionalization step, a fresh PBS 1x solution was streamed through *Inlet2* for at least 3 minutes in order to remove the physisorbed molecules. Finally, the flow was stopped and three transfers were recorded in the linear regime, measuring the device with the sensing gate. The concentrations of α-synuclein solution sensed were the following: 0.25 pM, 2.5 pM, 25 pM, 250 pM, 2.5 nM, 25 nM, 250 nM. Each sensing experiment started and finished with an electrical characterization by exploiting the reference gate electrode in order to cross-check the overall operation status of the organic semiconductor.

3. Results and discussion

3.1. Characterization of the sensing platforms

Anti-(α-synuclein) antibodies (Abs) have been tethered onto the polycrystalline Au by means of two different approaches, the so-termed "approach I" and "approach II" (Figure 1). The former relies on an amino-terminated pegylated thiol ($HSC_{11}EG_6NH_2$), whose amino groups have been successively activated with glutaraldehyde (Gl) (Betancor et al., 2006; Walt and Agayn, 1994). This leads to a functionalized Au extremely reactive towards primary amines, which are usually abundant in the Abs backbone (see Fig.1(top)). The second approach does not covalently graft the antibody to the surface but instead tethers it to the His-tagged recombinant Protein G (PG), which is anchored to the Au electrode. PG can target efficiently the crystallizable Ab region (Choe et al., 2016; Song et al., 2012; Young et al., 2005). Furthermore, PG is robustly anchored to the polycrystalline Au thanks to its His tag that exhibits an affinity towards different metals such as Ni and Au (Fig. 1(bottom)) (Iori et al., 2008; Yang and Zhao, 2007). Since there is not an

established protocol for tethering a bio-molecule onto a metal surface without affecting partially its bio-functionality, we pursued both approaches that have pros and cons and compared the outcomes of the sensing devices in order to establish the most suitable approach. For instance, approach I yields covalent albeit random Ab grafting, whereas approach II guarantees more oriented Ab immobilization onto the Au surface although non-covalent interactions are involved.

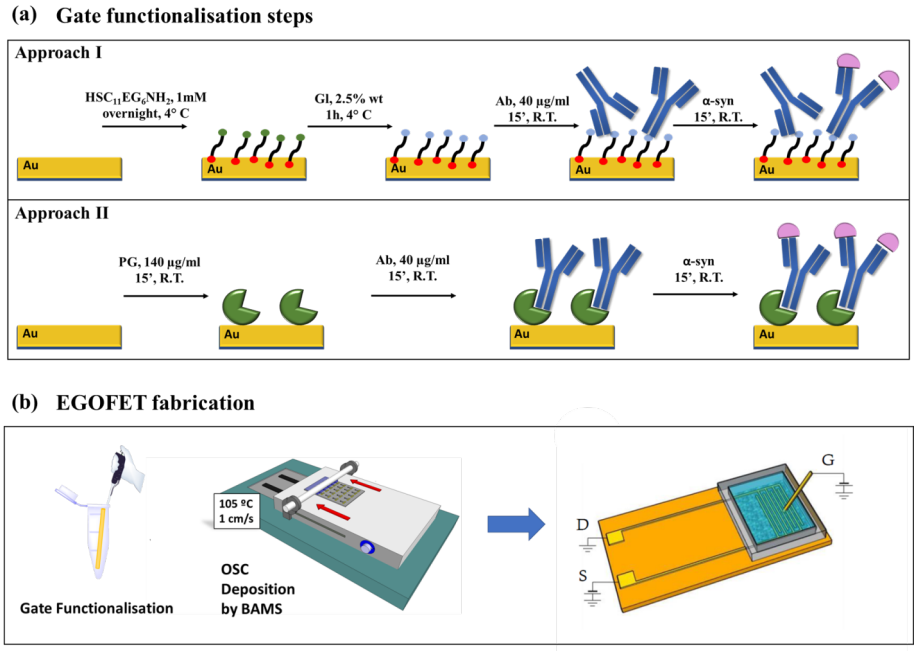

Figure 1. a) Scheme of the Au surface functionalization protocol with Approach (top) I and (bottom) II. b) Scheme of the EGOFET fabrication, including the gate functionalisation, organic semiconductor deposition and EGOFET implementation.

Our first goal was to verify the presence of the surface binders (*viz*. $HSC_{11}EG_6NH_2$-based SAM and PG), their reactivity towards Abs and, consequently, their sensitivity towards α-synuclein. Electrochemical means (i.e., electrochemical impedance spectroscopy, differential pulse voltammetry and cyclic voltammetry) were used for this purpose. The PG grafting yielded a pronounced area normalised R_{CT} increase (ΔR_{CT}) up to 20 kΩ/cm^2 and a consequent decrease of the current density (ΔJ) down to 440 μA/cm^2 (Fig.2a,b and Fig. S2 for the CV characterisation). As expected, the $HSC_{11}EG_6NH_2$-based SAM features higher ΔR_{CT} (~120 kΩ/cm^2) than PG due to its more ordered and compact packing onto the Au surface (see Fig.2c). Measurements by XPS and further electrochemical measurements support this evidence (see Fig.S3, S4, and S5, Supporting Information). Both functionalization approaches were successfully tested towards a 0.25 μM solution of α-synuclein proving their sensing ability towards this analyte. In particular, the two approaches exhibit opposite trends of the response with respect to Abs adsorption and detection of α-synuclein. The $HSC_{11}EG_6NH_2$-based SAM (i.e. higher coverage and molecular packing) showed an increase of ΔR_{CT} and a consequent ΔJ decrease (Fig.2d and Fig.S2) after being incubated with α-synuclein. Conversely, PG showed a decrease of ΔR_{CT} and a consequent ΔJ increase (i.e. lower coverage and molecular packing). Albeit it is beyond the scope of this paper, these experimental proofs hint at a relevant redistribution of the surface charge on the metal due to the pairs Ab-PG as well as Ab-PG-synuclein. Besides, the different responses could also be influenced by the Au SAM bond formation that leads to permanent electric dipoles.

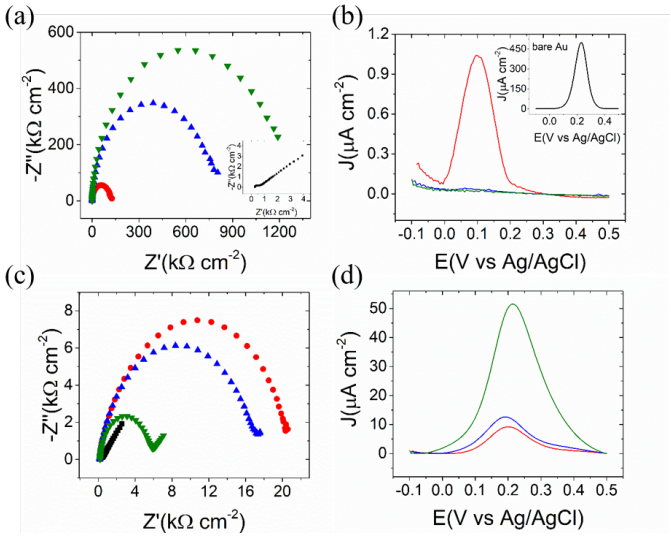

Figure 2. EIS and DPV characterization of the Ab functionalized surface. Approach I. (a) EIS: SAM-coated Au (red curve), Ab-SAM-coated Au (blue curve), after incubation in a solution of α-synuclein 0.25 μM (green curve). In the inset, the curve relative to pristine Au is represented, (b) DPV: SAM-coated Au (red line), Ab-SAM-coated Au (blue line), after incubation in a solution of α-synuclein 0.25 μM (green line). In the inset, the DPV of pristine Au is reported. Approach II. (c) EIS: bare Au (black curve), PG-coated Au (red curve), Ab-PG-coated Au (blue curve), after incubation in a solution of α-synuclein 0.25 μM (green curve). (d) DPV: PG-coated Au (red line), Ab-PG-coated Au (blue line), after incubation in a solution of α-synuclein 0.25 μM (green line).

In order to further characterize the functionalized substrates, we used surface plasmon resonance (SPR) to assess the two approaches on a planar Au film (Fig.3). As explained in the experimental section, the SPR is equipped with microfluidic channels that allow real-time monitoring of the absorption process. The excellent sensitivity of this technique allowed us to track the reflected light variation (*%ΔR*), which is directly related to the Au surface grafting. In particular, *ΔR* as a

function of time allows one to monitor the kinetics of this phenomenon. Apart from demonstrating the successful glutaraldehyde activation of $HSC_{11}EG_6NH_2$-based SAM in approach I, as well as the PG adsorption on gold in approach II, the transient ΔR change related to the surface functionalization with anti-(α-synuclein) Ab was monitored and exponentially fitted for both approaches (Ab concentration was fixed at 40μg/ml). Hence, the growth factors (f) were calculated (see Fig.S6, Supporting Information). It turned out that approach I was faster than approach II yielding f = 112 (±1) s and f = 212 (±1) s, respectively. Although a calibration curve and more advanced measurements would be required for achieving a quantitative analysis, it can be stated that approach II leads to the adsorption of more anti-(α-synuclein) Ab (ΔR = 12) with respect to approach I (ΔR = 6). Concerning the α-synuclein recognition (concentration selected equal to 250 nM), a larger ΔR is recorded for approach II with respect to approach I. Thus, these data do not only hint a larger amount of anti(α-synuclein) Ab in approach II, but also an improved control of Ab orientation onto the Au surface. In agreement with the electrochemistry results, SPR measurements confirm the successful Ab functionalization of the surfaces employing both approaches, as well as their capability to sense α-synuclein.

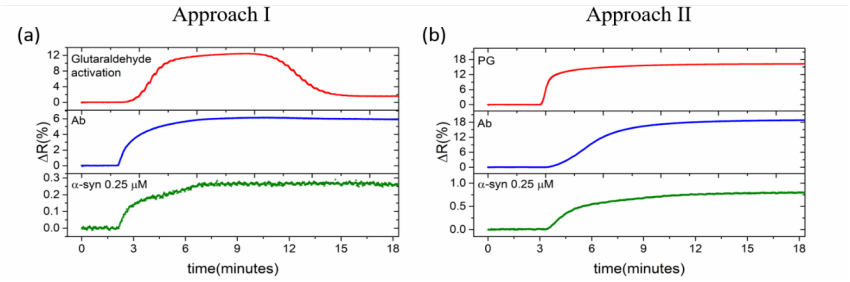

Figure 3. SPR characterization of the functionalized substrates:(a) approach I and (b) approach II.

3.2. Top-gated EGOFETs: α-synuclein detection

Since both approaches turned out to be extremely responsive towards α-synuclein, we employed them as gate terminals into a standard EGOFET architecture (see Fig.1b). This allows one to monitor the detection of α-synuclein by using a transistor. Concerning the general architecture of the device, we choose *Kapton®* as a flexible supporting substrate for the interdigitated electrodes. The channel area was coated by a thin-film blend composed of the organic semiconductor 2,8-Difluoro-5,11-bis(triethylsilylethynyl)anthradithiophene (diF-TES-ADT, Fig.4a) and polystyrene (PS) deposited by bar-assisted meniscus shearing (BAMS), as reported earlier (Fig.1b) (Del Pozo et al., 2016; Leonardi et al., 2018; Temiño et al., 2016; (Zhang et al., 2016). As previously published, the role of PS improves the general stability of the electrical performances, especially when operated in liquid (Campos et al., 2018; Leonardi et al., 2016; Paterson et al., 2016; Pérez-Rodríguez et al., 2018; Temiño et al., 2016b; Zhang et al., 2016a; Zhao et al., 2016). This is achieved due to the vertical phase separation of the two components that takes place during the deposition; in other terms, the organic semiconductor crystallizes sandwiched between a bottom PS layer and a top thin skin PS layer. Finally, the device was exposed to phosphate-buffered saline (PBS) solution at pH 7.2, where a top gate electrode was immersed, namely an Au wire (Fig. 1b).

The *I-V* transfer characteristics were acquired after the *ex-situ* functionalization of the gate with anti-(α-synuclein) Ab. Subsequently, the electrode was immersed in benchmark solutions of α-synuclein and, afterwards, implemented as a top gate electrode in the standard EGOFET layout (Fig.4a). This guaranteed no chemical and/or biological contamination onto the organic semiconductor surface. Prior to any sensing experiment, electrical conditioning was always performed (*i.e.*, V_{DS} and V_{GS} equal to -0.1 V for 20 minutes) and the *ex-situ* functionalization was verified step by step by recording at least three transfers for each step (Fig.4b,c). Aiming at

avoiding misleading interpretation, additional *I-V* transfer characteristics were acquired at the end of each sensing experiments by using a freshly cleaned Au wire (*viz*. gate electrode). This allowed us to verify if any extrinsic phenomena (such as bias stress or damaging of the semiconducting film) related to the device were contributing to the recorded trends (see Fig.S7, Supporting Information). These final cross-checks elucidated the direct interplay between the functionalization steps and the electrical changes occurring at the transistor. Two well-defined trends were observed corresponding to the two approaches. In particular, approach I shows a positive shift of the *I-V* transfer after exposure of the gate to an increasing concentration of α-synuclein, whereas approach II exhibits a negative one (Fig.4d,e, and Fig. S8, Supporting Information).

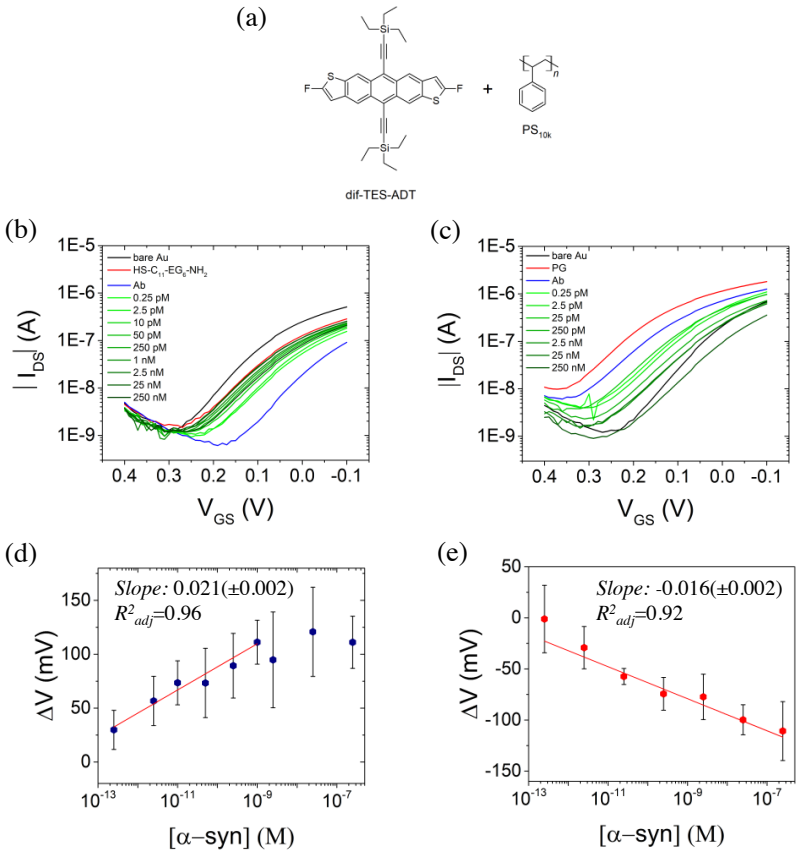

Figure 4. (a) Molecular structure of diF-TES-ADT and PS. *I-V* transfer characteristics of the EGOFET (V_{DS} = -0.1 V) with (b) Ab-SAM-coated Au gate (approach I) and (c) Ab-PG-coated Au gate (approach II), upon interaction with α-synuclein. The sensing response for both approaches in terms of ΔV is depicted, respectively, in (d) and (e) plots. The bar error is relative to three measurements.

As widely reported in the literature, an organic or biological coating assembled onto the gate surface or the semiconducting material can drastically affect the electrical performance of the transistor operated in aqueous media (Berto et al., 2017, 2016; Casalini et al., 2013; Loig Kergoat et al., 2012; Roberts et al., 2008; Torsi et al., 2013). The introduction of surface dipoles can either build-up an additional potential into the device or lead to a relevant change of the electrical double-layer capacitance. Aiming at a more quantitative description, we extracted the ΔV solely related to the bio-molecular recognition event regardless of the device-to-device variability, which affects usually the threshold voltage. For this reason, our data have been extracted by adopting the mathematical elaboration suggested by *Ishikawa et al*.(Duan et al., 2012; Ishikawa et al., 2009; Lee et al., 2011), as follows:

$$\Delta V = \frac{\Delta I}{g_{\mathrm{m}}}$$

where ΔI=($I_{DS,ini}$-$I_{DS,fin}$) is the difference between the $I_{DS,\mathrm{ini}}$ related to the device functionalized by the anti-(α-synuclein) Ab and the $I_{DS,fin}$ corresponding to a specific concentration of antigen, and g_m is the maximum transconductance (namely the first derivative of I_{DS} versus V_{GS}). In particular, it has been decided to verify our device sensitivity at the gate bias, where the g_m is the highest, namely -0.07 V (see Fig. S9, Supporting Information). At the end of the sensing experiments, approach I yields a shift of +111(±20) mV, while an opposite shift of -111(±29) mV is found in approach II. In accordance with the electrochemical data, our EGOFETs sensed two opposite trends corresponding to the two functionalization approaches (Fig.4d,e).

Concerning approach I, the sensing trend can be explained by considering the outer charges arising from the α-synuclein (Hammock et al., 2013). As reported in the literature, α-synuclein has an

isoelectric point (pI) equal to 4.67, thus it is negatively charged at physiological pH (*viz*. pH > pI) (Gould et al., 2014). As a result, a *p*-doping effect takes place due to an increase of negative charges onto the gate electrode. This leads to an extra accumulation of positive charge carriers into the conductive channel of diF-TES-ADT. Furthermore, the response ranges from 0.25 pM to 1 nM featuring a sensitivity equal to 21(±2) mV/dec. On the contrary, a rationalization based on simply the PI of α-synuclein does not hold for approach II due to the presence of different biomolecules on the surface. In this case, the sensing range appears wider than in approach I, namely from 0.25 pM to 250 nM, with a sensitivity of -16(±2) mV/dec. In other terms, both approaches reveal similar sensitivities, but approach II reached two orders of magnitude higher the upper limit of the sensitivity range. This outcome is consistent with the SPR assays, which qualitatively pointed to a more efficient Au electrode for the detection of α-synuclein in approach II. Furthermore, both approaches show comparable LOD values, namely at sub-pM concentration. This high sensitivity makes these devices well-suited to study pathological versus physiological levels of this biomarker (Lee et al., 2006).

3.3. Coplanar gating: in-situ (bio)-functionalization

Although top-gated architecture allowed us to verify the sensibility of our functionalized EGOFET, this technology can be solely used at the laboratory scale for proof-of-concept. Aiming at more sound technology, a coplanar gate architecture is demanded along with a well-suited microfluidic cell for the sample handling. The coplanar architecture improves intrinsically the electrical characterization of such a device, because it exerts an ideal control of the gate area immersed in the aqueous solution. Furthermore, it allows a straightforward implementation to more sophisticated circuitry, because no mobile electrodes are used like the Au wire in the top gate architecture. In our case, we designed two planar gates termed “reference” and “sensing” (Fig.5a).

According to this layout, we manufactured a microfluidic cell composed of two well-defined chambers, so-termed “chamber 1” and “chamber 2”. The former contains the reference gate along with the source/drain electrodes covered by the organic semiconductor, whereas the latter hosts the sensing gate. These chambers are joined together by a “connecting channel”, whose role is fundamental for the overall functioning of this self-standing chip (Fig.5a). This connecting channel guarantees the electrical connection between the sensing gate and the organic semiconductor through the electrolyte media. Furthermore, it enables to inject the sample containing α-synuclein or antibodies in “chamber 1” avoiding the cross-contamination of the organic semiconductor. In other terms, chamber 1 together with the connecting channel are always filled by phosphate buffer, and chamber 2 is filled with different solutions (as mentioned in the experimental part, section 2.8). The use of peristaltic pumps together with the narrow section of the connecting channel guarantees the proper functioning of the chip. This has been experimentally verified by using the reference electrode to characterize the electrical performance of the organic semiconductor at the beginning as well as at the end of the sensing experiments (Fig.S10, Supporting Information). In the Supporting Information, it is included a video showing that no cross-contamination occurs between the two chambers when “chamber 1” is filled up with a dye solution (Video 1, Supporting Information).

The scheme of the microfluidic device has been validated with finite element analysis to calculate the velocity field and the concentration of α-synuclein within the geometric spaces occupied by the solution during infilling of either buffer solution or biological sample (see Supporting Information for further details). Navier Stokes equation for momentum balance and convection-diffusion equation for the transport of dilute species have been solved in combined iterations with Comsol Multiphysics ®, in order to account for the dependence of viscosity on concentration and

evaluate the time-dependent evolution of the analyte concentration. The velocity field of the solution inside the chamber with the functionalized gate is plotted in Fig.5c, where it is possible to appreciate the unperturbed state of the chamber above the interdigitated electrodes. The boundary condition for the flow rate, set by the peristaltic pumps (10 μl/min), is inducing a velocity field showing the maximum intensity near the widening section of the inlet, with a parabolic like profile decaying towards the sides of the microfluidic chamber. Due to laminarity, the streamlines extracted by simulation show that the fluid in the connecting channel between the two chambers is not displaced by the injection of the sample. The evolution in time of the α-synuclein concentration within the simulated geometry is plotted in Fig.5d. The resulting concentration of the α-synuclein is affected by convection and diffusion within the sensing chamber, whereas the only diffusion is controlling the front advancing towards the chamber of the interdigitated electrodes. After 10 minutes from the injection, the value of α-synuclein concentration resulting from the simulation is negligible in the volume of the solution above the interdigitated electrodes, while it is equal to sample concentration above the functionalized gate. The geometry occupied by the electrolyte has been simulated also for evaluating electrostatic potential distribution between the functionalized gate and interdigitated electrodes (Poisson equation) with electrical permittivity reported for PBS buffer solution (i.e., V_{GS}= -0.6 V). The calculated contour of potential across the connecting channel is reported in Fig. 5e.

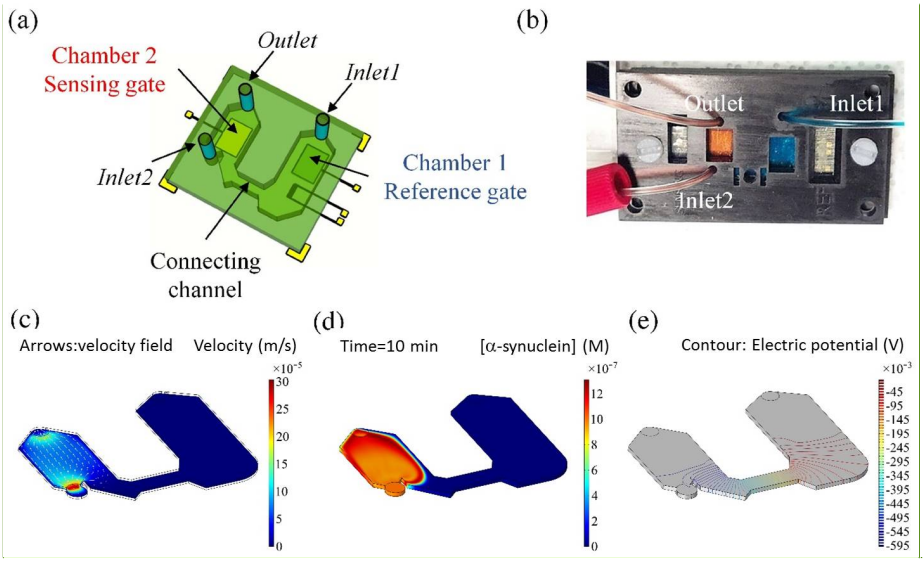

Commented [sr1]: Marta perdón, pequeña cosa, la letra de la figura está cubierta
Creo que no la tengo yo esta

Figure 5. (a) 3D scheme of the microfluidic setup. (b) Real image of the microfluidic setup filled with red and blue dyes, the sensing chamber and the device chamber, respectively (see video and more details in SI). (c) Velocity field inside the microfluidics during sample injection resulting from finite element simulation. (d) Concentration of α-synuclein within Chamber 2 after 10 minutes from the injection. (e) Potential contour plot in electrolyte between sensing gate and interdigitated electrodes.

Coplanar architecture in microfluidics was tested using approach I. The sensing gate was *in-situ* functionalized (see experimental part for more details, section 2.8). Subsequently, the sensing experiments were also performed *in-situ* by injecting the α-synuclein solutions for 5 minutes and then rinsing 3 minutes with the electrolyte media (see Experimental section). The *I-V* transfer

characteristics were acquired by spanning the gate-source voltage from 100 mV to -400 mV and with a V_{DS} = -0.1 V. (Fig.6a). The data turned out to be coherent with the previous experiments related to the top gated EGOFETs. As a result, positive doping was observed by increasing the α-synuclein concentrations in the range 0.25 pM-25 nM, reaching a LOD of 0.25 pM, ΔV value as high as +166(±52) mV and a slight increase in sensitivity (37(±5) mV/dec) with respect to the top gated devices (Fig.6b and Fig.S11, Supporting Information). Although future work should be devoted to test biological fluid samples, a high selectivity can be envisaged due to the high binding affinity between the Ab used with α-synuclein (Kumar et al., 2020).

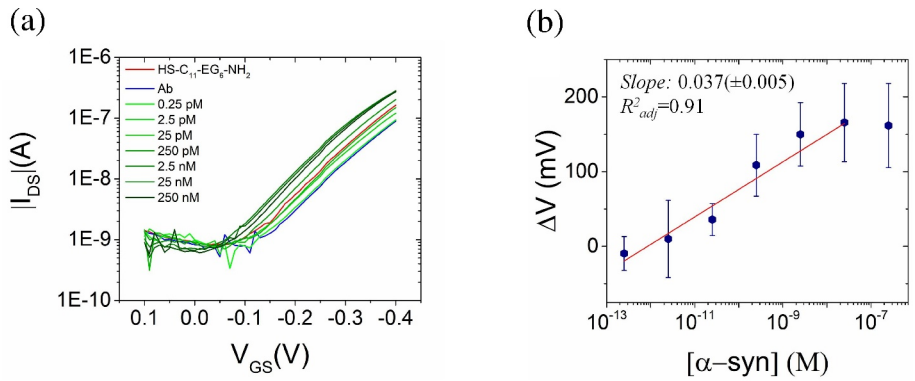

Figure 6. (a) Transfer characteristics (V_{DS} = -0.1 V) of the sensing experiment employing the EGOFET with Ab-SAM-coated coplanar-gate Au gate and (b) relative calibration curve.

4. Conclusions

A sensing platform based on a dual gate coplanar electrolyte-gated organic field-effect transistor in a microfluidic chamber has been demonstrated to detect α-synuclein, a hallmark of neurodegeneration in important pathologies like Parkinson's and Alzheimer's down to LOD equal to 0.25 pM. The optimum immuno-detection strategy based on anti-(α-synuclein) monoclonal antibody was inferred by a comparative study of two surface functionalization routes of the gate electrode. Both showed similar sensitivities and LOD values, but they showed different response range, namely approach II had a wider range than approach I (*viz*. 0.25 pM - 250 nM versus 0.25 pM - 1 nM, respectively). The microfluidics layout has been designed to avoid cross-contamination between the sensing gate and the organic semiconductor. Such an approach allowed us the *in-situ* functionalization of the sensing gate and the electrical tests with reference solutions of α-synuclein. The herein reported devices combine the high sensitivity and short measurement tests, with the electrical readout and the simplicity and upscaling compatibility of the fabrication methods employed (see Table S1 for a collection of the figures of merit of state-of-the-art α-synuclein sensors which have been described). Thus, these devices showed excellent potential for the prognostics and diagnosis of synucleinopathies such as PD, and also can provide a promising label-free tool for gaining insights into the role of α-synuclein and its aggregation mechanism, which is pivotal for a comprehensive understanding of such neurodegenerative diseases. Future work will be devoted to fabricate technologically more advanced devices to validate them in a larger set of samples and test our label-free sensors using real samples from patient's fluids.

Acknowledgments

This work was funded by the EXPLORA project MAT2015-72760-EXP and ERC StG 2012-306826 e-GAMES. The authors also thank the DGI (Spain) project FANCY CTQ2016-80030-R and GENESIS PID2019-111682RB-I00, the Generalitat de Catalunya (2017-SGR-918), the Networking Research Center on Bioengineering, Biomaterials, and Nanomedicine (CIBER-BBN) and the Spanish Ministry of Economy and Competitiveness, through the "Severo Ochoa" Programme for Centers of Excellence in R&D (SEV-2015-0496). S. R. acknowledges FPU Fellowship from the Ministry and is enrolled in the PhD program of the Universitat Autònoma of Barcelona (UAB). The research leading to these results has also received funding from the People Programme (Marie Curie Actions) of the Seventh Framework Programme of the European Union (FP7/2007-2013) under Research Executive Agency Grant Agreement No. 600388 (TECNIOSpring programme), and from the Agency for Business Competitiveness of the Government of Catalonia, ACCIÓ. The Surface Plasmon Resonance (SPR) measurements were performed through the ICTS NANBIOSIS platform, more specifically in the Biodeposition and Biodetection Unit of the CIBER in Bioengineering, Biomaterials & Nanomedicine (CIBER-BBN) at the Catalan Institute of Nanoscience and Nanotechnology (ICN2). The microfluidic device design and fabrication were performed with funding from the European Union's Horizon 2020 research and innovation programme under the Marie Skłodowska-Curie grant agreement 764281 (AiPBAND), and Marie Skłodowska-Curie grant agreement 813863 (BORGES).

References

Bard, A.J., Faulkner., L.R., 2002. Electrochemical Methods: Fundamentals and Applications, America.

Berto, M., Casalini, S., Di Lauro, M., Marasso, S.L., Cocuzza, M., Perrone, D., Pinti, M.,

Cossarizza, A., Pirri, C.F., Simon, D.T., Berggren, M., Zerbetto, F., Bortolotti, C.A., Biscarini, F., 2016. Biorecognition in organic field effect transistors biosensors: The role of the density of states of the organic semiconductor. Analytical Chemistry 88, 12330–12338.

Berto, M., Diacci, C., D'Agata, R., Pinti, M., Bianchini, E., Lauro, M. Di, Casalini, S., Cossarizza, A., Berggren, M., Simon, D., Spoto, G., Biscarini, F., Bortolotti, C.A., 2017. EGOFET Peptide Aptasensor for Label-Free Detection of Inflammatory Cytokines in Complex Fluids. Advanced Biosystems 2, 1700072.

Berto, M., Vecchi, E., Baiamonte, L., Condò, C., Sensi, M., Di Lauro, M., Sola, M., De Stradis, A., Biscarini, F., Minafra, A., Bortolotti, C.A., 2019. Label free detection of plant viruses with organic transistor biosensors. Sensors and Actuators, B: Chemical 281, 150–156.

Betancor, L., López-Gallego, F., Hidalgo, A., Alonso-Morales, N., Dellamora-Ortiz, G., Mateo, C., Fernández-Lafuente, R., Guisán, J.M., 2006. Different mechanisms of protein immobilization on glutaraldehyde activated supports: Effect of support activation and immobilization conditions. Enzyme and Microbial Technology 39, 877–882.

Bougea, A., Stefanis, L., Paraskevas, G.P., Emmanouilidou, E., Vekrelis, K., Kapaki, E., 2019. Plasma alpha-synuclein levels in patients with Parkinson's disease: a systematic review and meta-analysis. Neurological Sciences 40, 929–938.

Campana, A., Cramer, T., Simon, D.T., Berggren, M., Biscarini, F., 2014. Electrocardiographic recording with conformable organic electrochemical transistor fabricated on resorbable bioscaffold. Advanced Materials 26, 3874–3878.

Campos, A., Riera-Galindo, S., Puigdollers, J., Mas-Torrent, M., 2018. Reduction of Charge Traps

and Stability Enhancement in Solution-Processed Organic Field-Effect Transistors Based on a Blended n-Type Semiconductor. ACS Applied Materials and Interfaces 10, 15952–15961.

Casalini, S., Dumitru, A.C., Leonardi, F., Bortolotti, C.A., Herruzo, E.T., Campana, A., Oliveira, R.F. De, Cramer, T., Garcia, R., Biscarini, F., 2015. Multiscale Sensing of Antibody À Antigen Interactions by Organic Transistors and Single-Molecule Force Spectroscopy. ACS Nano 9, 5051–5062.

Casalini, S., Leonardi, F., Cramer, T., Biscarini, F., 2013. Organic field-effect transistor for label-free dopamine sensing. Organic Electronics 14, 156–163.

Chang, Chun Wei, Yang, S.Y., Yang, C.C., Chang, Chia Wen, Wu, Y.R., 2020. Plasma and Serum Alpha-Synuclein as a Biomarker of Diagnosis in Patients With Parkinson's Disease. Frontiers in Neurology 10, 1–7.

Choe, W., Durgannavar, T.A., Chung, S.J., 2016. Fc-binding ligands of immunoglobulin G: An overview of high affinity proteins and peptides. Materials 9, 994.

Cramer, T., Chelli, B., Murgia, M., Barbalinardo, M., Bystrenova, E., De Leeuw, D.M., Biscarini, F., 2013. Organic ultra-thin film transistors with a liquid gate for extracellular stimulation and recording of electric activity of stem cell-derived neuronal networks. Physical Chemistry Chemical Physics 15, 3897–3905.

Del Pozo, F.G., Fabiano, S., Pfattner, R., Georgakopoulos, S., Galindo, S., Liu, X., Braun, S., Fahlman, M., Veciana, J., Rovira, C., Crispin, X., Berggren, M., Mas-Torrent, M., 2016. Single crystal-like performance in solution-coated thin-film organic field-effect transistors. Advanced Functional Materials 26, 2379–2386.

Desbief, S., Casalini, S., Guerin, D., Tortorella, S., Barbalinardo, M., Kyndiah, A., Murgia, M., Cramer, T., Biscarini, F., Vuillaume, D., 2016. Electrolyte-gated organic synapse transistor interfaced with neurons. Organic Electronics 38, 21–28.

Duan, X., Li, Y., Rajan, N.K., Routenberg, D.A., Modis, Y., Reed, M.A., 2012. Quantification of the affinities and kinetics of protein interactions using silicon nanowire biosensors. Nature Nanotechnology 7, 401–407.

Engvall, E., Perlmann, P., 1971. Enzyme-linked immunosorbent assay (ELISA) quantitative assay of immunoglobulin G. Immunochemistry 8, 871–874.

Goedert, M., Jakes, R., Spillantini, M.G., 2017. The Synucleinopathies: Twenty Years on. Journal of Parkinson's Disease 7, S51–S69.

Gould, N., Mor, D.E., Lightfoot, R., Malkus, K., Giasson, B., Ischiropoulos, H., 2014. Evidence of native α-synuclein conformers in the human brain. Journal of Biological Chemistry 289, 7929–7934.

Guo, J., 2016. Uric Acid Monitoring with a Smartphone as the Electrochemical Analyzer. Analytical Chemistry 88, 11986–11989.

Guo, J., Ai, Y., Cheng, Y., Li, C.M., Kang, Y., Wang, Z., 2015. Volumetric measurement of human red blood cells by MOSFET-based microfluidic gate. Electrophoresis 36, 1862–1865.

Hammock, M.L., Knopfmacher, O., Naab, B.D., Tok, J.B.H., Bao, Z., 2013. Investigation of protein detection parameters using nanofunctionalized organic field-effect transistors. ACS Nano 7, 3970–3980.

Huang, X., Xu, D., Chen, J., Liu, J., Li, Y., Song, J., Ma, X., Guo, J., 2019. Smartphone-based analytical biosensors. Anales de la Quimica 143, 5339–5351.

Iori, F., Corni, S., Felice, R.D., 2008. Unraveling the interaction between histidine side chain and the Au(111) surface: A DFT study. Journal of Physical Chemistry C 112, 13540–13545.

Ishikawa, F.N., Curreli, M., Chang, H., Chen, P., Zhang, R., Cote, R.J., Thompson, M.E., Zhou, C., 2009. A Calibration Method for Nanowire Biosensors to Suppress Device-to-Device Variation. ACS Nano 3, 3969–3976.

Jonsson, A., Inal, S., Uguz, L., Williamson, A.J., Kergoat, L., Rivnay, J., Khodagholy, D., Berggren, M., Bernard, C., Malliaras, G.G., Simon, D.T., 2016. Bioelectronic neural pixel: Chemical stimulation and electrical sensing at the same site. Proceedings of the National Academy of Sciences 113, 9440–9445.

Kaisti, M., 2017. Detection principles of biological and chemical FET sensors. Biosensors and Bioelectronics 98, 437–448.

Kergoat, L., Herlogsson, L., Braga, D., Piro, B., Pham, M.C., Crispin, X., Berggren, M., Horowitz, G., 2010. A water-gate organic field-effect transistor. Advanced Materials 22, 2565–2569.

Kergoat, Loïg, Piro, B., Berggren, M., Horowitz, G., Pham, M.C., 2012. Advances in organic transistor-based biosensors: From organic electrochemical transistors to electrolyte-gated organic field-effect transistors. Analytical and Bioanalytical Chemistry 402, 1813–1826.

Kergoat, Loig, Piro, B., Berggren, M., Pham, M.C., Yassar, A., Horowitz, G., 2012. DNA detection with a water-gated organic field-effect transistor. Organic Electronics 13, 1–6.

Kumar, S.T., Jagannath, S., Francois, C., Vanderstichele, H., Stoops, E., Lashuel, H.A., 2020. Characterization and validation of 15 α-synuclein conformation-specific antibodies using well-characterized preparations of α-synuclein monomers, fibrils and oligomers with distinct structures and morphology: How specific are the conformation-specific α-syniclein antibodies. bioRxiv 1–54. DOI: 10.1101/2020.06.15.151514

Lee, B.Y., Sung, M.G., Lee, J., Baik, K.Y., Kwon, Y.K., Lee, M.S., Hong, S., 2011. Universal parameters for carbon nanotube network-based sensors: Can nanotube sensors be reproducible? ACS Nano 5, 4373–4379.

Lee, P.H., Lee, G., Park, H.J., Bang, O.Y., Joo, I.S., Huh, K., 2006. The plasma alpha-synuclein levels in patients with Parkinson's disease and multiple system atrophy. Journal of Neural Transmission 113, 1435–1439.

Leonardi, F., Casalini, S., Zhang, Q., Galindo, S., Gutiérrez, D., Mas-Torrent, M., 2016. Electrolyte-Gated Organic Field-Effect Transistor Based on a Solution Sheared Organic Semiconductor Blend. Advanced Materials 28, 10311–10316.

Leonardi, F., Tamayo, A., Casalini, S., Mas-Torrent, M., 2018. Modification of the gate electrode by self-assembled monolayers in flexible electrolyte-gated organic field effect transistors: Work function: Vs. capacitance effects. RSC Advances 8, 27509–27515.

Macchia, E., Manoli, K., Holzer, B., Di Franco, C., Ghittorelli, M., Torricelli, F., Alberga, D., Mangiatordi, G.F., Palazzo, G., Scamarcio, G., Torsi, L., 2018. Single-molecule detection with a millimetre-sized transistor. Nature Communications 9.

Magliulo, M., De Tullio, D., Vikholm-Lundin, I., Albers, W.M., Munter, T., Manoli, K., Palazzo,

G., Torsi, L., 2016. Label-free C-reactive protein electronic detection with an electrolyte-gated organic field-effect transistor-based immunosensor. Analytical and Bioanalytical Chemistry 408, 3943–3952.

Magliulo, M., Mallardi, A., Mulla, M.Y., Cotrone, S., Pistillo, B.R., Favia, P., Vikholm-Lundin, I., Palazzo, G., Torsi, L., 2013. Electrolyte-gated organic field-effect transistor sensors based on supported biotinylated phospholipid bilayer. Advanced Materials 25, 2090–2094.

Parkula, V., Berto, M., Diacci, C., Patrahau, B., Di Lauro, M., Kovtun, A., Liscio, A., Sensi, M., Samorì, P., Greco, P., Bortolotti, C.A., Biscarini, F., 2020. Harnessing Selectivity and Sensitivity in Electronic Biosensing: A Novel Lab-on-Chip Multigate Organic Transistor. Analytical Chemistry.

Paterson, A.F., Treat, N.D., Zhang, W., Fei, Z., Wyatt-Moon, G., Faber, H., Vourlias, G., Patsalas, P.A., Solomeshch, O., Tessler, N., Heeney, M., Anthopoulos, T.D., 2016. Small Molecule/Polymer Blend Organic Transistors with Hole Mobility Exceeding 13 cm2V−1s−1. Advanced Materials 28, 7791–7798.

Pérez-Rodríguez, A., Temiño, I., Ocal, C., Mas-Torrent, M., Barrena, E., 2018. Decoding the vertical phase separation and its impact on C8-BTBT/PS Transistors properties. ACS Applied Materials & Interfaces 10, 7296–7303.

Rivnay, J., Inal, S., Salleo, A., Owens, R.M., Berggren, M., Malliaras, G.G., 2018. Organic electrochemical transistors. Nature Reviews Materials 3, 17086.

Roberts, M.E., Mannsfeld, S.C.B., Queralto, N., Reese, C., Locklin, J., Knoll, W., Bao, Z., 2008. Water-stable organic transistors and their application in chemical and biological sensors.

Proceedings of the National Academy of Sciences 105, 12134–12139.

Shi, M., Zabetian, C.P., Hancock, A.M., Ginghina, C., Hong, Z., Yearout, D., Chung, K.A., Quinn, J.F., Peskind, E.R., Galasko, D., Jankovic, J., Leverenz, J.B., Zhang, J., 2010. Significance and confounders of peripheral DJ-1 and alpha-synuclein in Parkinson's disease. Neuroscience Letters 480, 78–82.

Song, H.Y., Zhou, X., Hobley, J., Su, X., 2012. Comparative study of random and oriented antibody immobilization as measured by dual polarization interferometry and surface plasmon resonance spectroscopy. Langmuir 28, 997–1004.

Spillantini, M.G., Goedert, M., 2000. The Alpha-Synucleinopathies : Parkinson's Disease, Dementia with Lewy Bodies, and Multiple. Annals New York Academy of Sciences 920, 16–27.

Temiño, I., Del Pozo, F.G., Ajayakumar, M.R., Galindo, S., Puigdollers, J., Mas-Torrent, M., 2016. A Rapid, Low-Cost, and Scalable Technique for Printing State-of-the-Art Organic Field-Effect Transistors. Advanced Materials Technologies 1, 1–7.

Torsi, L., Farinola, G.M., Marinelli, F., Tanese, M.C., Omar, O.H., Valli, L., Babudri, F., Palmisano, F., Zambonin, P.G., Naso, F., 2008. A sensitivity-enhanced field-effect chiralsensor. Nature Materials 7, 412–417.

Torsi, L., Magliulo, M., Manoli, K., Palazzo, G., 2013. Organic field-effect transistor sensors: A tutorial review. Chemical Society Reviews 42, 8612–8628.

Twohig, D., Nielsen, H.M., 2019. α -synuclein in the pathophysiology of Alzheimer ' s disease. Molecular Neurodegeneration 14, 1–19.

Van De Burgt, Y., Lubberman, E., Fuller, E.J., Keene, S.T., Faria, G.C., Agarwal, S., Marinella, M.J., Alec Talin, A., Salleo, A., 2017. A non-volatile organic electrochemical device as a low-voltage artificial synapse for neuromorphic computing. Nature Materials 16, 414–418.

Walt, D.R., Agayn, V.I., 1994. The chemistry of enzyme and protein immobilization with glutaraldehyde. TrAC - Trends in Analytical Chemistry 13, 425–430.

Wang, N., Yang, A., Fu, Y., Li, Y., Yan, F., 2019. Functionalized Organic Thin Film Transistors for Biosensing. Accounts of Chemical Research 52, 277–287.

Wennström, M., Surova, Y., Hall, S., Nilsson, C., Minthon, L., Boström, F., Hansson, O., Nielsen, H.M., 2013. Low CSF Levels of Both α-Synuclein and the α-Synuclein Cleaving Enzyme Neurosin in Patients with Synucleinopathy. PLoS ONE 8.

Xu, D., Huang, X., Guo, J., Ma, X., 2018. Biosensors and Bioelectronics Automatic smartphone-based micro fl uidic biosensor system at the point of care. Biosensors and Bioelectronic 110, 78–88.

Xu, K., Zhou, R., Takei, K., Hong, M., 2019. Toward Flexible Surface-Enhanced Raman Scattering (SERS) Sensors for Point-of-Care Diagnostics. Advanced Science 6, 1900925.

Yang, Z., Zhao, Y.P., 2007. Adsorption of His-tagged peptide to Ni, Cu and Au (1 0 0) surfaces: Molecular dynamics simulation. Engineering Analysis with Boundary Elements 31, 402–409.

Young, M.B., Oh, B.K., Lee, W., Won, H.L., Choi, J.W., 2005. Study on orientation of immunoglobulin G on protein G layer. Biosensors and Bioelectronics 21, 103–110.

Zeng, F., Duan, W., Zhu, B., Mu, T., Zhu, L., Guo, J., 2019. Paper-Based Versatile Surface-

Enhanced Raman Spectroscopy Chip with Smartphone-Based Raman Analyzer for Point-of-Care Application. Analytical Chemistry 91, 1064–1070.

Zhang, Q., Leonardi, F., Casalini, S., Temiño, I., Mas-Torrent, M., 2016. High performing solution-coated electrolyte-gated organic field-effect transistors for aqueous media operation. Scientific Reports 6, 1–10.

Zhao, K., Wodo, O., Ren, D., Khan, H.U., Niazi, M.R., Hu, H., Abdelsamie, M., Li, R., Li, E.Q., Yu, L., Yan, B., Payne, M.M., Smith, J., Anthony, J.E., Anthopoulos, T.D., Thoroddsen, S.T., Ganapathysubramanian, B., Amassian, A., 2016. Vertical Phase Separation in Small Molecule:Polymer Blend Organic Thin Film Transistors Can Be Dynamically Controlled. Advanced Functional Materials 26, 1737–1746.